Impact of heavy hole levels on the photovoltaic conversion efficiency of In Ga1–N/InN quantum dot intermediate band solar cells

A. El Aouami, K. Feddi, M. El Haouari, M. El Yadri, N. Ben Afkir, M. Zazoui, E. Feddi, C.A. Duque, F. Dujardin

Version of Record: https://www.sciencedirect.com/science/article/pii/S0749603619302496
Manuscript_c27e0f9cb3841f5157a0098072bee147

Impact of heavy hole levels on the photovoltaic conversion efficiency of $In_xGa_{1-x}N/InN$ quantum dot intermediate band solar cells

A. El Aouami[a], K. Feddi[b,c], M. El Haouari[a,d], M. El Yadri[a], N. Ben Afkir[e], M. Zazoui[e], E. Feddi[a], C. A. Duque[f], F. Dujardin[g,*]

[a] *Laboratoire de Matière Condensée et Sciences Interdisciplinaires (LaMCScI), Group of Optoelectronic of Semiconductors and Nanomaterials, ENSET, Mohammed V University in Rabat, Morocco.*
[b] *REAM Laboratory, UIR, Rabat, Morocco.*
[c] *EIMIS Laboratory, FST, University Abdelmalek Essadi, Tanger, Morocco.*
[d] *Centre Régional des Métiers de l'Education et de Formation (CRMEF), Tanger, Morocco.*
[e] *Laboratory of Condensed Matter and Renewable Energy, Faculty of Sciences and Technology, University Hassan II of Casablanca, BP146, Mohammedia, Morocco.*
[f] *Grupo de Materia Condensada-UdeA, Instituto de Física, Facultad de Ciencias Exactas y Naturales, Universidad de Antioquia, Calle 70 No. 52-21, Medellín, Colombia.*
[g] *Université de Lorraine, LCP-A2MC, F-57000 Metz, France.*

Abstract

We report a theoretical investigation of the photovoltaic conversion efficiency of solar cells based on the introduction of $In_xGa_{1-x}N/InN$ quantum dot supracrystals arrayed in the i-region of a $p-i-n$ photodiode. The position and width of intermediate bands induced by the discrete quantized energy levels of electrons and holes originating from QDs are determined by using the Kronig-Penney model. Thus, interband and intersubband transitions are determined for different dot sizes and inter-dot distances. Taking into account the hole level and its impact on the band offset usually neglected

*Corresponding author
Email address: francis.dujardin@univ-lorraine.fr (F. Dujardin)

in the same studies, all characteristic parameters of the cell such as open circuit voltage, short circuit current density and photoelectric conversion efficiency are determined as a function of the In-concentration, mean size and inter-dot spacing of QDs. The results show that the performances of this new generation of solar cell increase considerably and can be adjusted by controlling the size, inter-dot spacing and In-concentration.
Keywords: Solar cells; photovoltaic; quantum dots; intermediate band; conversion efficiency; temperature effect.

---

1. Introduction

Since the pioneering studies of Luque, Marti, Levy and Nozik [1–3] the concept of a new generation of solar cells lives a real proliferation. Going beyond the limit of Shockley-Queisser [4] by increasing the photovoltaic conversion efficiency (η) up to 30% remains a challenge for both scientists and industrial. Attempts of doping semiconductors with impurities in order to create intermediate levels in the gap did not give very satisfactory results. Progress in the field of nanotechnology, mainly the mastery of growth techniques of nanomaterials, have allowed the implementation of quantum dots (QDs) at the junction between two semiconductors. Thus, intermediate quantized levels can take place in the forbidden zone. The direct effect of this intermediate band is to reduce the non-radiative transitions often encountered in the doping phenomenon and consequently makes this technology very promising with the hope of going beyond the conventional limit and thus lowering the cost of electricity produced by the photovoltaic technology.

In order to introduce our study, let us present a short overview of the

main works that have been developed in this theme (for more details, we invite the reader to see the references [5-7]). The principle of the Quantum Dot Intermediate Band Solar Cell (QD-IBSC) such as described by Luque *et al.* [1] is that the photons with less energy than the band gap can contribute in the photoelectric process of the material via a two-step process: valence band (VB) $\rightarrow$ intermediate band (IB) $\rightarrow$ conduction band (CB), thereby increasing the short-circuit current without degrading the open-circuit voltage. Consequently, theoretically, the QD-IBSC has a higher value of conversion efficiency than a traditional solar cell with only valence band and conduction band, and therefore attracts much attention of researchers.

Lazarenkova and Balandin [8] have studied the band structure in a three dimensional quantum dot array. They have shown a possible engineering of mini-bands by changing the size, inter-dot space and the magnitude of barrier confinement. Using this description, Shao *et al.* [9] implemented an IBSC and showed that this structure enhances the photoelectric process and the carrier transport. Their first-principle semi-analytical treatment allows to obtain the optimum dimensions for a maximum efficiency in the case of $InAs_{0.9}N_{0.1}/GaAs_{0.98}Sb_{0.02}$ QDs. Levy *et al.* [10] give a qualitative study of some systems (QD/barrier/substrate). They have shown that under some conditions on the band offsets of the three materials, the efficiency can reach 60%. Bailey *et al.* [11] have shown that ten-layer $InAs/GaAs$ quantum dot solar cells exhibit enhanced short-circuit current and open circuit voltage in comparison with a $GaAs$ $p-i-n$ solar cell. Aroutiounian *et al.* [12] suggested the introduction of QDs in the intrinsic region of a $p-i-n$ photodiode. They calculated the photo-current by solving the minority carrier

transport equation. It has been deduced that the conversion efficiency can be significantly increased by insertion of self-organized QDs into the intrinsic region. Their performance can be controlled by adjusting their quantized energy levels according to the size and the shape of the $InAs$ islands. More recently, a detailed balance photovoltaic theory has been used to determine the solar cells efficiency [13]. The authors proposed a method to control the band flatness of the intermediate band in $InAs/GaAs$ QDSC via the doping. Their results show that the efficiency can reach 44.92%.

The theoretical analysis of the intermediate bands generated by the arrangement of the QDs in the three directions is difficult. So, many authors use the Kronig-Penney model [14] based on the periodicity of the confinement potential. The studies [15–18] have explored the IBSC in the case of $InN/In_xGa_{1-x}N$ quantum dots embedded in the intrinsic region of a $p-i-n$ solar cell. The intermediate band of the electrons was obtained by solving the Schrödinger equation using the Kronig-Penney model. These studies are complementary and prove that this process increases the photoelectric conversion efficiency up to 61.7% by manipulating the concentration of indium, the size of the dots and the inter-dot distance. $InAsN/GaAsSb$ QDs-IBSC have been also the subject of a study [19] using the Kronig-Penney model. In this this type of materials, their calculation shows that the efficiency can reach 70%.

We note that in all these studies the authors have neglected the intermediate band of the holes. Indeed, as remarked by the first predictors of this model [10], the conversion efficiency depends strongly of the positions of the intermediate bands of both electrons and holes.

In this study, we consider a InN quantum dot embedded inside the p($InGaN$)-i(InN-QDs)-n($InGaN$) junction, and take into account the confinement potential due to valence band offset. Using the Kronig-Penney model, we solve the Schrödinger equation of one particle in a $InGaN/InN$ QD by considering the temperature effects. We determine the position and the width of the intermediate band (IB), interband (VB $\rightarrow$ IB) and intersubband (IB $\rightarrow$ CB) transitions in a $In_xGa_{1-x}N/InN$ QD solar cell. The solar cell characteristic parameters such as the conversion efficiency (η), the open circuit voltage (V_{oc}), and the short circuit current density (J_{oc}) of $In_xGa_{1-x}N/InN$ QD-IBSCs are determined. Therefore the effects of the temperature (T), mean size (L), inter-dot spacing (H), and In-content (x) on the position and width of IB are clearly analyzed. The organization of the paper is the following: Section II contains the presentation of the theoretical framework, in Section III, we discuss the obtained results and, in Section IV, the conclusions are given.

2. Theoretical framework

For a slight description, let us consider a lattice of cubic InN quantum dots (well) embedded in a $In_xGa_{1-x}N/InN$ matrix (barrier). The structure is immersed in the I-region of a $p-i-n$ photodiode. As indicated in Fig. 1, the structure looks like a periodic super-crystal structure admitting $D = L + H$ as period. H and L represent respectively the sizes of InN QDs and $InGaN$ regions in each direction (X, Y or Z axis).

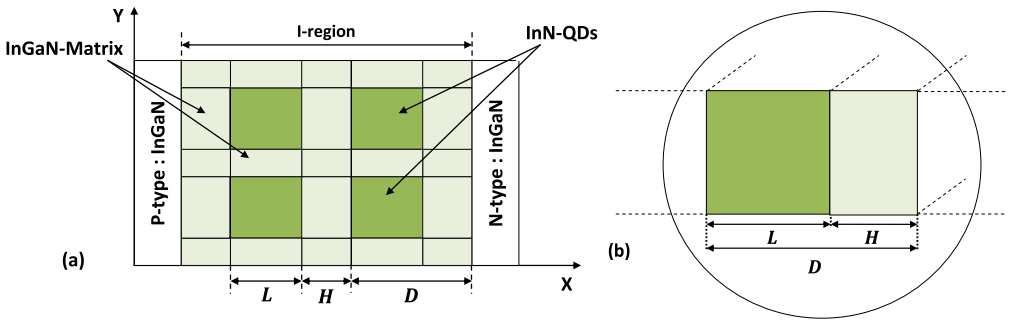

Figure 1: Schematic of $p-i-n$ type $InGaN/InN$ QD-IBSC in the XY plane. The green cubes represent the InN QDs narrow gap material as potential well embedded in the $InGaN$ matrix with broad gap potential barrier (a); zoom on the i-region where L, H and D denote respectively the size of InN QDs, the inter-dot distance and the super-crystal period (b).

The Schrödinger equation describing one particle ground state energy inside a cubic quantum dot (CQD) can be expressed as:

$$\mathcal{H}\Psi(X,Y,Z) = E\Psi(X,Y,Z) \tag{1}$$

Due to the symmetry of the problem, the 3D envelope wave function $\Psi(X,Y,Z)$ can be written as a product of three 1D eigenfunctions ψ_{k_i}:

$$\Psi(X,Y,Z) = \Pi\psi_{k_i}(i), \quad \text{with } i = X,Y,Z \tag{2}$$

and the total energy spectrum E is the sum of the 1D-eigenvalues:

$$E = \sum E_i(k_i) \tag{3}$$

k_i is the wave vector of the quasi-free particle in a periodic structure, it is defined by:

$$k_i = \frac{2\pi n_i}{\mathcal{N}D}, \quad n_i = 0, \pm1, \pm2, \pm3, ..., \pm\frac{\mathcal{N}}{2} \tag{4}$$

$\mathcal{N}$ is a large integer. Since X, Y and Z axis are equivalent, the total energy can be written as $E = 3E_X(\frac{2\pi n_X}{\mathcal{N}D})$, so we can limit ourselves to the

X direction. Within the framework of the effective mass approximation, the temperature (T) and In-concentration (x) dependent Hamiltonian of a single electron in a QD can be written in the X direction as:

$$\mathcal{H} = -\frac{\hbar^2}{2}\nabla_X \left(\frac{1}{m_e^*(x,T)}\nabla_X\right) + V^w(x,T) \tag{5}$$

The one direction confinement potential is given by [8]:

$$V^w(x,T) = \begin{cases} 0\,, & \text{if } \ 0 \leq X \leq L/2 \\ V_{0e}(x,T)\,, & \text{if } \ L/2 < X < L/2 + H \end{cases} \tag{6}$$

The height of the potential barrier in the conduction band is assumed to depend on the temperature T and the composition x according to:

$$V_{0e}(x,T) = 0.7 * [E_g(In_xGa_{1-x}N,T) - E_g(InN,T)] \tag{7}$$

In relation (5), $m_e^*(x,T)$ is the temperature and In-concentration dependent electron effective mass, it is given by:

$$m_e^*(x,T) = \begin{cases} m_{InN}^*(T) & \text{if } \ 0 \leq X \leq \frac{L}{2} \\ x.m_{InN}^*(T) + (1-x)\, m_{GaN}^*(T) & \text{if } \frac{L}{2} < X < \frac{L}{2} + H \end{cases} \tag{8}$$

The temperature dependent electron effective mass for GaN or InN is obtained by considering the relation [20]:

$$m_A^*(T) = \left[1 + \frac{C}{E_g(A,T)}\right] m_0 \tag{9}$$

where m_0 is the free electron mass, A represents GaN or InN. C is obtained from the previous equation at $T = 300\,K$ with $m_A^*(T = 300\,K) = [0.19(1 - x) + 0.1x]^{-1} m_0$. The temperature dependence of the band-gap energy for GaN and InN materials is given by the Varshni relation [21]:

$$E_g(A,T) = E_g(A,0) - \frac{\alpha T^2}{T + \beta} \tag{10}$$

where $E_g(A,0)$ is the gap of a given semiconductor A at $T=0$. The band-gap energy of ternary alloy $In_xGa_{1-x}N$ is approximately represented by a quadratic function of Indium concentration as [22]:

$$E_g(In_xGa_{1-x}N,T) = xE_g(InN,T)+(1-x)E_g(GaN,T)-1.43\,x(1-x)\ \ (eV) \tag{11}$$

According to the classical Kronig-Penney model, the solutions of the Schrödinger equation (1) in one direction can be obtained by solving the well known dispersion relation for electrons as well as for holes . So, for electron bound states, $0 < E_X < V_{0e}(x,T)$, the relation writes as [8]:

$$\cos(k_i D) = \cos(k^w L)\cosh(k^b H) - \frac{1}{2}\left(\frac{k^w m^*_{InGaN}(T)}{k^b m^*_{InN}(T)} - \frac{k^b m^*_{InN}(T)}{k^w m^*_{InGaN}(T)}\right)\sin(k^w L)\sinh(k^b H) \tag{12}$$

and for unbound states, $E_X \geq V_{0e}(x,T)$, the relation becomes:

$$\cos(k_i D) = \cos(k^w L)\cos(k^b H) - \frac{1}{2}\left(\frac{k^w m^*_{InGaN}(T)}{k^b m^*_{InN}(T)} + \frac{k^b m^*_{InN}(T)}{k^w m^*_{InGaN}(T)}\right)\sin(k^w L)\sin(k^b H) \tag{13}$$

The parameters k^b and k^w are respectively:

$$k^b = \frac{\sqrt{2m^*_{InGaN}(T)\,[V_{0e}(x,T) - E_X]}}{\hbar} \tag{14}$$

and

$$k^w = \frac{\sqrt{2m^*_{InN}(T)\,E_X}}{\hbar} \tag{15}$$

In order to obtain the position and width of minibands in the potential well, the right side of formula (12) can be expressed as a function $f(E_X)$ of energy E_X:

$$f(E_X) = \cos(k^w L)\cosh(k^b H) - \frac{1}{2}\left(\frac{k^w m^*_{InGaN}(T)}{k^b m^*_{InN}(T)} - \frac{k^b m^*_{InN}(T)}{k^w m^*_{InGaN}(T)}\right)\sin(k^w L)\sinh(k^b H) \tag{16}$$

Similarly, for the potential barrier the right side of formula (13) can be written as:

$$f(E_X) = \cos(k^w L)\cos(k^b H) - \frac{1}{2}\left(\frac{k^w m^*_{InGaN}(T)}{k^b m^*_{InN}(T)} + \frac{k^b m^*_{InN}(T)}{k^w m^*_{InGaN}(T)}\right)\sin(k^w L)\sin(k^b H) \tag{17}$$

Knowing that $|\cos(k_i D)| \leqslant 1$, the region of absolute values $|f(E_X)| \leqslant 1$ should correspond to different values of the energy E_X which determine the possible minibands in the barrier or in the well. For example, for $x = 0.35$ and $T = 300\,K$, Eq.(7) leads to $V_{0e} = 0.985\,eV$. Fig. 2 shows the positions and the widths of the first minibands for $L = 3\,nm$ and $H = 1\,nm$. The first miniband corresponds to $0.177\,eV < E_X < 0.294\,eV$, i.e. $0.530\,eV < E_e < 0.881\,eV$ so that it is located in the well and its width is $\Delta_e = 0.351\,eV$. However, the second corresponds to $0.874\,eV < E_X < 1.330\,eV$, i.e. $2.621\,eV < E_e < 3.989\,eV$ so that it is located in the barrier. The same method is used to obtain the equivalent equations and minibands for the holes. In this study, we consider only the electron and hole energies extracted from the first minibands.

Let us recall the most important parameters of a solar cell photo-diode; the IBSCs are characterized by a net photo-generated current density J_{sc} given by [1]:

$$\frac{J_{sc}}{q} = [\mathcal{F}(E_{13}, \infty, T_s, 0) - \mathcal{F}(E_{13}, \infty, T_c, U_{cv})] + [\mathcal{F}(E_{23}, E_{12}, T_s, 0) - \mathcal{F}(E_{23}, E_{12}, T_c, U_{ci})] \tag{18}$$

where $T_s = 6000\,K$ and $T_c = 300\,K$ are the surface temperatures of the sun and the solar cell, respectively. q is the elementary charge, U_{cv} (U_{ci}) is the chemical potential between CB and VB, (IB and CB). The transition energies for bound states E_{13}, E_{12}, and E_{23}, labelled in Fig. 3 can be obtained from

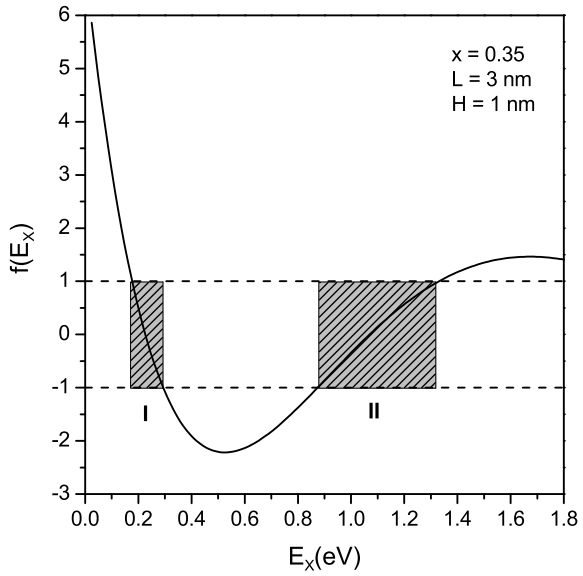

Figure 2: Function $f(E_X)$ of electron versus E_X for $x = 0.35$, $L = 3\,nm$ and $H = 1\,nm$. The intersection of $f(E_X)$ with the lines -1 and $+1$ determines the minibands: I is the miniband in the well, II represents the first miniband in the barrier potential.

the dispersion relation (16). We note that the flux of photons absorbed or emitted by a semiconductor is given by Roosbroeck-Shockley relation [23]:

$$\mathcal{F}(E_l, E_u, T, U) = \frac{2\pi}{h^3 c^2} \int_{E_l}^{E_u} \frac{E^2 dE}{\exp\left(E - U\right)/kT - 1} \tag{19}$$

where E_l and E_u are the lower and upper energy limits, respectively, c is the light speed in vacuum, k is the Boltzmann constant, and U is the chemical potential. On the other hand, for a p-i-n solar cell, the output voltage V_{oc} of a IBSC can be expressed as [24]:

$$V_{oc} = U_{cv} = U_{ci} + U_{iv} \tag{20}$$

U_{ci} and U_{iv} are given by the expressions [16]:

$$U_{ci} = E_{23} + 0.5\,\Delta_e - E_C + E_{FC} \tag{21}$$

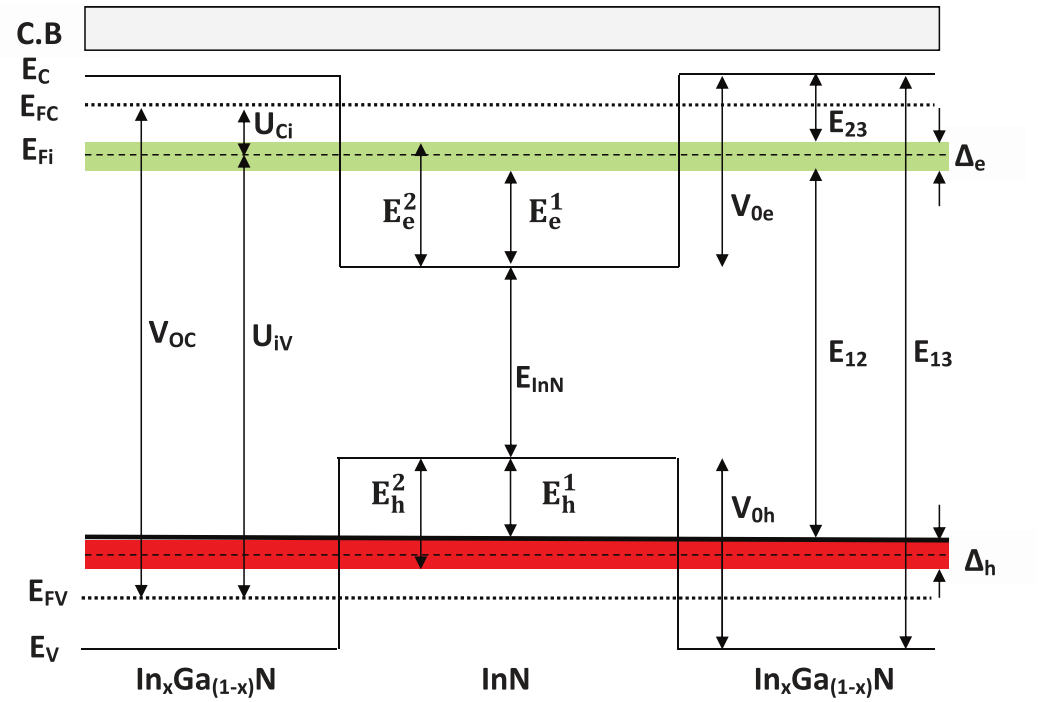

Figure 3: Energy band diagram of $In_xGa_{1-x}N/InN$ single intermediate band solar cell, where E_C and E_V denote the energies of CB and VB of the host material and E_{13} represents its bandgap while E_{InN} is the band gap of InN. V_{0e} and V_{0h} are the band offsets. E_j^1 and E_j^2 are the boundaries of the mini-band of particle j ($j = e, h$). Δ_e and Δ_h are respectively the IB widths of electron and hole. E_{12} and E_{23} are respectively the energies of bottom and top sub-gaps. E_{FC}, E_{FV} and E_{FI} are the quasi-Fermi levels of CB, VB and IB. Finally, U_{iv} and U_{ci} are the chemical potential between VB and IB on the one hand, IB and CB on the other hand.

$$U_{iv} = E_{12} + 0.5\,\Delta_e - E_{FV} + E_V + V_{0h} - E_h^1 \tag{22}$$

Δ_e is shown in Fig. 3, it represents the width of IB. E_{FC} and E_{FV} are the quasi Fermi levels of CB and VB respectively given by [15, 25]:

$$E_C - E_{FC} = kT\ \ln\frac{N_C}{n} \tag{23}$$

$$E_{FV} - E_V = kT\ \ln\frac{N_V}{p} \tag{24}$$

where N_C and N_V denote effective conduction band density and effective va-

lence band density, respectively. n and p are the charge carrier concentration of electrons and holes respectively. The electron and hole concentrations are inversely proportional to the volume of $InGaN$ QD. They can be assumed to be $n = p = 10^{-5}/V_{InGaN}$ with $V_{InGaN} = (L + H)^3 - L^3$.

The four parameters that characterize the performance of a photovoltaic cell are: the short circuit current (I_{sc}), the open-circuit voltage (V_{oc}), the fill factor (FF), and the conversion efficiency (η). The fill factor is also a function of V_{oc} and I_{sc}. It is defined as the ratio of maximum power that can be extracted from a solar cell to the ideal power. It is represented in terms of percentage such as $FF = (V_m\, I_m)/(V_{oc}\, I_{sc})$ where V_m and I_m correspond to the operating point of the I-V characteristic that maximizes the output power. In the present study we consider the ideal case by assuming $FF = 1$. Therefore, the efficiency of the IBSC is defined as:

$$\eta = \frac{V_{oc}\, J_{sc}\, FF}{P_{in}} = \frac{V_{oc}\, J_{sc}}{P_{in}}. \tag{25}$$

where $P_{in} = \sigma T^4$ is the incident power per unit area coming from the sun and $\sigma = 5.67 \times 10^{-8}\, Wm^{-2}K^{-4}$ is the Stefan-Boltzmann constant.

3. Results and discussion

Following the previous description given in Fig. 3, the different energy transitions E_{12}, E_{23} and E_{13}, photo-generated current density (J_{sc}), output voltage (V_{oc}) and photovoltaic conversion efficiency (η) of $In_xGa_{1-x}N/InN$ QD-IBSCs are investigated. The recent physical parameters of these materials are listed in Table 1 [22, 26]. We recall that all previous studies [15, 16] considered only the transitions involving the top of the valence band. They also ignored the temperature dependence of the gap and of the masses of the

charge carriers. So, to be more realistic, we take into account in this study the hole levels located in the valence band offset of the junction $InGaN/InN$ (red band in Fig. 3) and the temperature dependencies.

Table 1: Physical parameters used in the present calculations.

$Parameters$	GaN	InN
m_e^*/m_0	0.193	0.054
m_h^*/m_0	0.810	0.835
$Eg(0)(eV)$	3.3	0.6
$\alpha(meV/K)$	0.593	0.245
$\beta(K)$	600	624
$N_V(cm^{-3})$	$8 * 10^{15}T^{3/2}$	$10^{16}T^{3/2}$
$N_C(cm^{-3})$	$2.3 * 10^{14}T^{3/2}$	$1.76 * 10^{14}T^{3/2}$

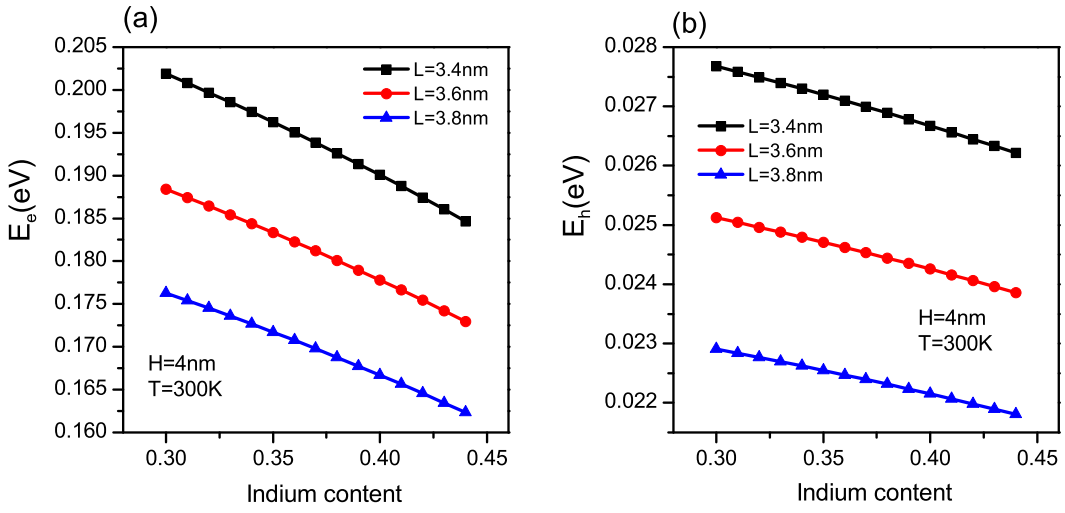

Figure 4: Ground state energies of electron (a) and hole (b) as functions of the Indium content x for $H = 4\,nm$ and different QD size values: $L = 3.4$, 3.6, and $3.8\,nm$.

We start our analysis by investigating the influence of the Indium content x on the fundamental energies of the electron in IB (E_e) and heavy hole in valence band offset (E_h). The IB in conduction and valence bands can

be determined by solving Kronig-Penney equations given by Eq.(16) and Eq.(17) for the electron and hole. Fig. 4(a) and Fig. 4(b) present the variation of the ground state energies of the electron (E_e) and hole (E_h) against the In-concentration (x) for $T = 300\,K$ and $H = 2\,nm$. As we can see, E_e and E_h decrease with increasing x. On the other hand for a fixed x, a decreasing of the ground state energy is observed as the size of the InN-QDs increases. This is a consequence of quantum confinement effects. Fig. 5(a) shows the optical transitions E_{12}, E_{23} and E_{13} versus the In-

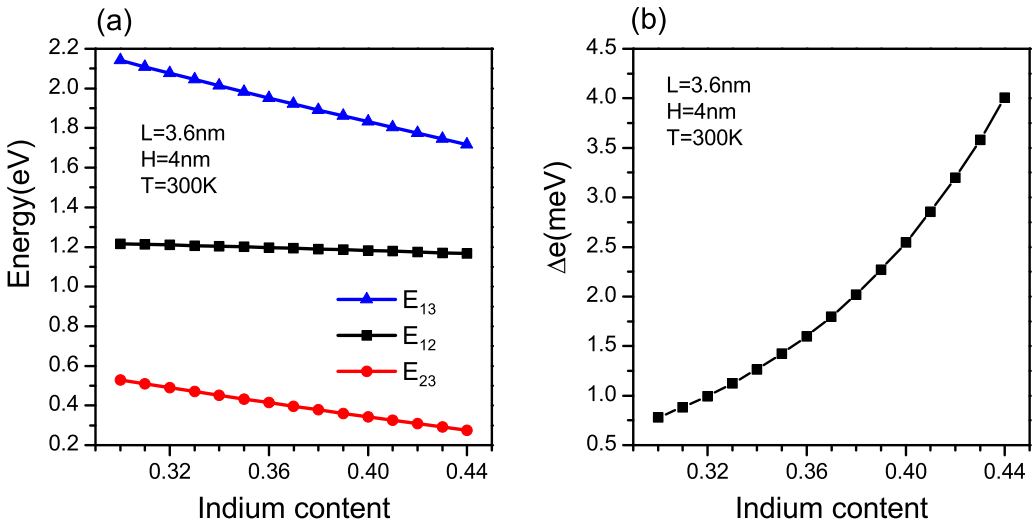

Figure 5: Variation of the band gap E_{13}, sub-bands E_{12} and E_{23} (a), IB width (b) at fixed $L = 3.6\,nm$, $H = 4\,nm$ and $T = 300\,K$, versus In-concentration x.

content (x) for $T = 300\,K$, $L = 3.6\,nm$ and $H = 4\,nm$. The curves show that the intersubband ground state transition between the intermediate and the conduction bands (IB→CB) E_{23}, and the host band gap E_{13} obtained by considering the hole level, decrease while x increases. However, the inter-band transition energy from the hole level to intermediate band E_{12}, decreases

slightly with the In-content x. The same behaviours have been observed by Zhang *et al.* [16] and Deng *et al.* [15]. Fig. 5(b) shows the variation of the IB width (Δ_e) versus the In-content (x) for fixed $L = 3.6\,nm$, $H = 4\,nm$ and $T = 300\,K$. We can remark that the augmentation of the In-concentration enlarges the width of IB which leads to an increasing of the absorption of long-wave sun radiation. This effect will have a positive impact on the solar cell efficiency.

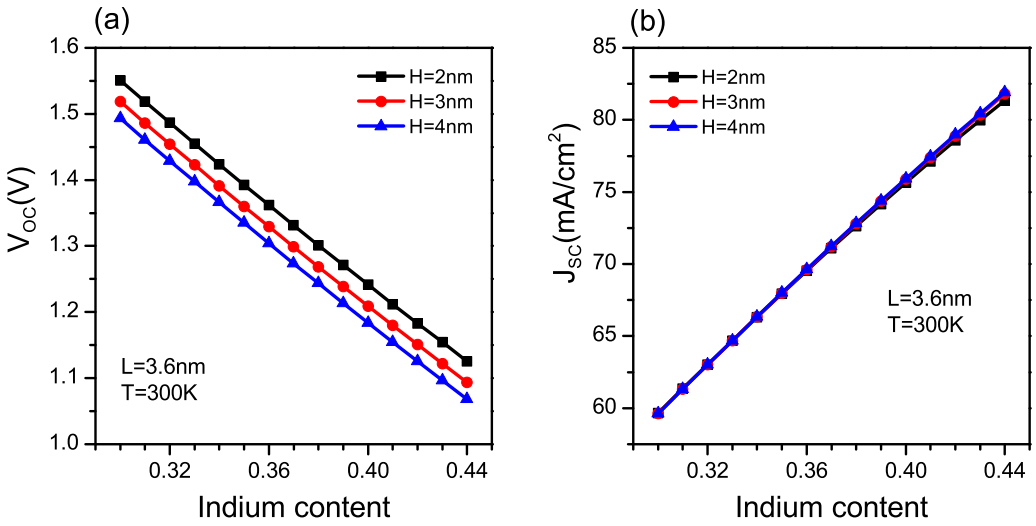

Figure 6: Open-circuit voltage variation as a function of In-content x (a) and photo-generated current density variation versus In-concentration (b). The dot size and the temperature are fixed at $L = 3.6\,nm$ and $T = 300\,K$, respectively and the inter-dot spacing takes three values: $H = 2, 3$ and $4\,nm$.

Fig. 6(a) presents the open-circuit voltage (V_{oc}) as a function of x for $T = 300\,K$, $L = 3.6\,nm$ and for different values of $H = 2, 3$ and $4\,nm$. It shows that the V_{oc} is strongly dependent on the variation of x and the QD sizes. For a given H the V_{oc} decreases linearly with the concentration x, this is due to the diminution of the host gap of $In_xGa_{1-x}N$ barrier.

To understand the correlation between all parameters influencing the efficiency, we present in Fig. 6(b) the J_{sc} versus x for $T = 300\,K$, $L = 3.6\,nm$ and for different values of $H = 2, 3$ and $4\,nm$. As we can see the photocurrent density J_{sc}, computed from the expressions (18) and (19), increases by increasing the In-content x. Fig. 7 presents the photovoltaic conversion

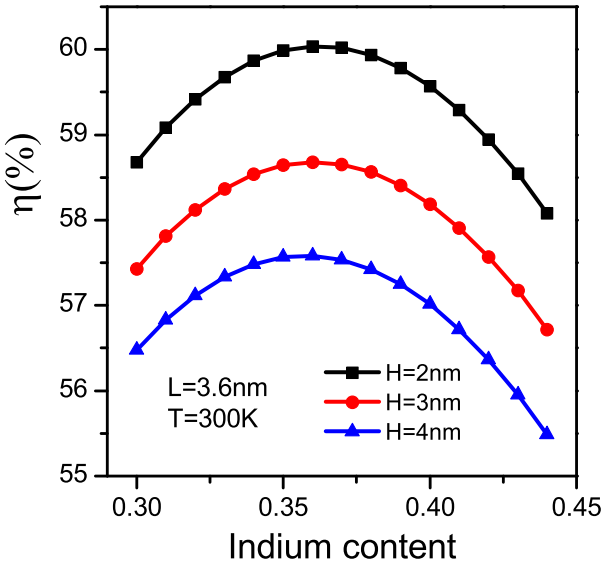

Figure 7: Photovoltaic conversion efficiency as function of the In-content x for different values of the inter-dot spacing size $H = 2$, 3 and $4\,nm$ and for a fixed InN-dot size $L = 3.6\,nm$.

efficiency (η) as a function of the Indium content x for $T = 300\,K$, $L = 3.6\,nm$ and for several values of the $InGaN$ inter-dot size $H = 2, 3$ and $4\,nm$. Under extremely favorable conditions, when the maximum power can be extracted from the solar cell, which corresponds to the ideal filling factor $FF = 1$, we can notice that whatever the In-content x, the best efficiencies are obtained for reduced inter-dot distances ($H = 2\,nm$). Our curves show that, for $L = 3.6\,nm$, the maximum efficiency reaches 60.03% for $x = 0.36$ and for

$H = 2\,nm$. In order to compare our results with those of previous studies, we recall that Zhang *et al.* [16] found a maximum efficiency of 59.79%. The improvement of our results is attributed to the fact that Zhang *et al.* have neglected the true band offset introduced by the confinement hole levels and the temperature dependence of the band gap energy and of effective masses of electron and hole. Thus, taking into account the real transitions between the holes and electrons levels corresponding to the forbidden band of the QD influences the performances of the solar cells and makes it possible to improve the yields for all dot sizes.

Now let us discuss the influence of the inter-dot spacing H on the photovoltaic conversion efficiency. Fig. 8(a) presents the energy transitions E_{12} and E_{23} as functions of L for $T = 300\,K$, $H = 2\,nm$ and $x = 0.34$. We note that the transition E_{12} and the IB width (Fig. 8b) decrease while increasing L, which can be interpreted by the effect of low quantum confinement in wider QDs. As depicted in Fig. 8(c), for a given H and x the V_{oc} is

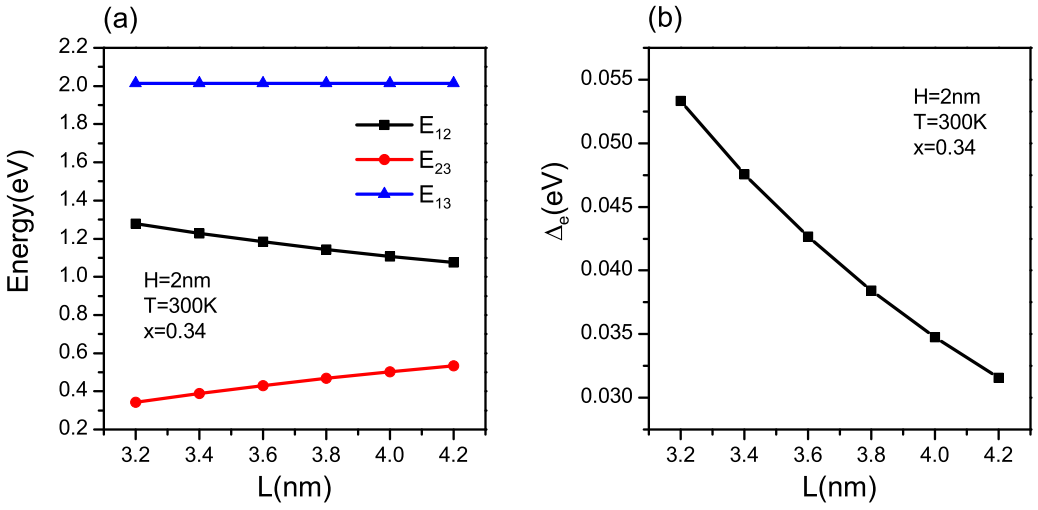

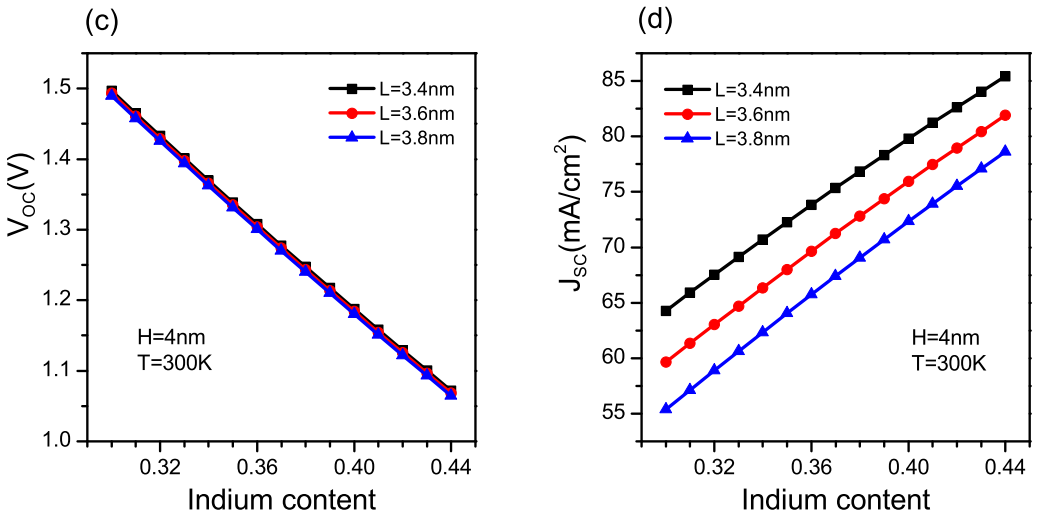

Figure 8: Variation of the sub-gap , E_{12} and E_{23} versus x at fixed $H = 2\,nm$, $T = 300\,K$ and $x = 0.34$ (a). IB width versus the InN-dot size L for a fixed $x = 0.34$ and $H = 2nm$ (b). Open-circuit voltage variation as a function of In-content (c). Photo-generated current density variation versus Indium-concentration (d). In (b) and (c) the inter-dot spacing and the temperature are fixed at $H = 4\,nm$ and $T = 300\,K$, respectively and the dot size takes different values: $L = 3.4$, 3.6, and $3.8\,nm$.

less dependent on L contrary to the dependence on the inter-dot distance H, this is because the transition E_{13} is not affected by the variation of the dot size as shown in Fig. 8(a). In Fig. 8(d), the variation of J_{sc} versus x for a given L shows that it increases monotonically with increasing x and its intensity is more pronounced for the strong confinement regime. Indeed, the increment of the J_{sc} is due to two main effects: the absorption of low-energy photons resulting to the reduction of the band gap due to In-concentration (x), and the existence of the intermediate band that allows the recuperation of electrons of lower energies [17]. Fig. 9 gives the representation of the efficiency η versus the In-content x for $T = 300\,K$, $H = 4\,nm$ and for three values of InN-dot size $L = 3.4$, 3.6 and $3.8\,nm$. As we can remark, the

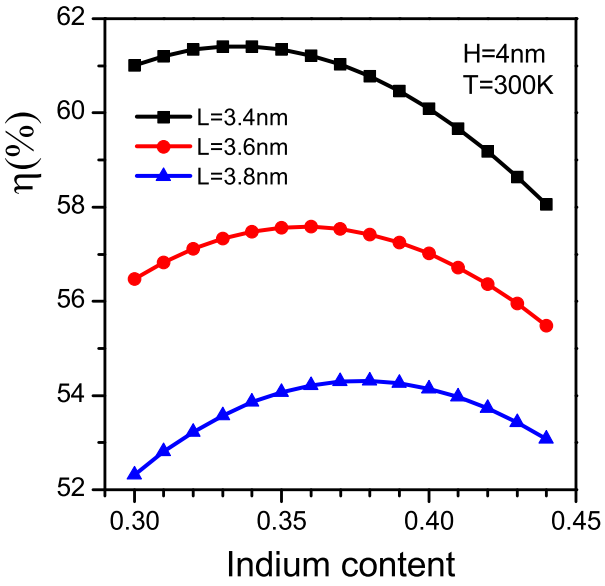

Figure 9: Photovoltaic conversion efficiency as function of the In-content x for $T = 300\,K$, $H = 4\,nm$, and for different values of the dot size $L = 3.4$, 3.6, $3.8\,nm$.

maximum of the efficiency reaches $\eta = 61.40\,\%$ for $x = 0.34$. The conversion efficiency is more important for small inter-dot distances. This results can be explained by the fact that the width of intermediate bands IB increases due to the orbital overlaps of charge carriers (electrons and holes) which are more important for low inter-dot spacing H. To analyse the influence of the temperature T on the maximum of the efficiency, we present in Fig. 10, the variations in the maximum performance of the QDSC as a function of temperature and taking into account the dot sizes and inter-dot distances. As shown in Fig. 10(a) and Fig. 10(b), the maximum of η decreases linearly with increasing T independently of H and L. As in tandem solar cells, this behaviour is attributed to the strong decreasing of the open voltage V_{oc} with increasing T.

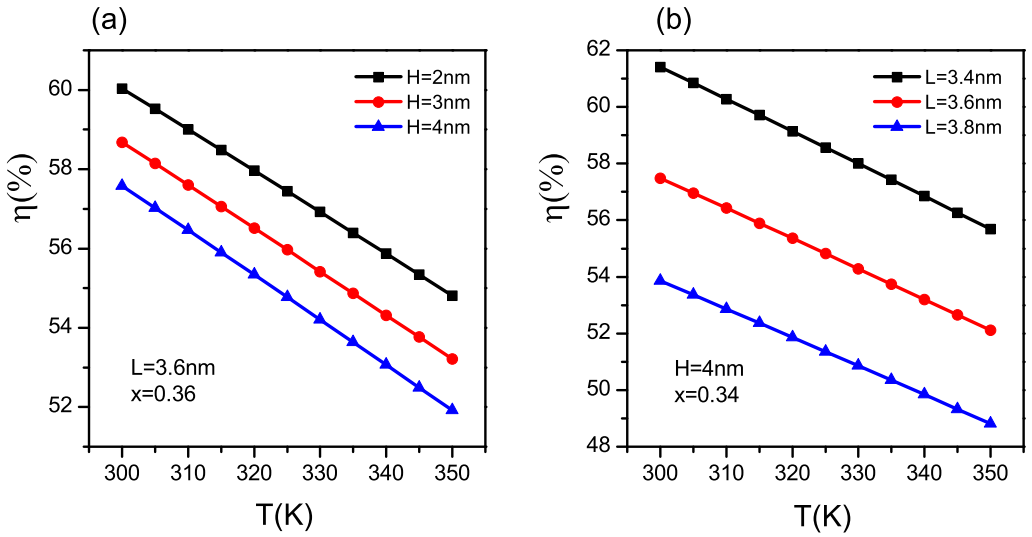

Figure 10: Variation of the maximum of photovoltaic efficiencies as function of the temperature T corresponding to the characteristic value of In-concentrations $x = 0.36$ and InN-dot size $L = 3.6$ nm for three inter-dot spacing values: $H = 2$, 3 and 4 nm (a), and for $x = 0.34$, $H = 4$ nm and three values of InN-dot sizes $L = 3.4$, 3.6 and 3.8nm (b).

4. Conclusion

Using the Kronig-Penney model and taking into account the hole levels located in the valence band offset, we have investigated the single intermediate-band solar cells of $In_xGa_{1-x}N/InN$ quantum dot super-crystals subjected to temperature effects. The characteristic parameters of the cell have been studied. Our analysis shows that the size of the quantum dots remains a determining factor for the short-circuit current density, while the spacing between the dots is the main factor controlling the open-circuit voltage. The main result of our approach is that the maximum performance of solar cells can be adjusted by controlling electron and hole levels via dot size, interdot spacing and indium concentration. Photovoltaic efficiency is linearly dependent on the filling factor FF, which reflects the efficiency of light absorp-

tion. In this study we have considered ideal conditions of light absorption ($FF = 1$). Objectively, we point out that the actual yields are relatively low compared to those obtained in this study because of the fill factor, which significantly reduces the value of the solar conversion.

5. References

[1] A. Luque and A. Marti, " Increasing the Efficiency of Ideal Solar Cells by Photon Induced Transitions at Intermediate Levels," Phys. Rev. Lett, vol. 78, no. 26, pp. 5014-5017, 1997.

[2] A. Marti, L. Cuadra and A. Luque, " Quantum dot intermediate band solar cell," 28th IEEE PVSC, pp. 940-943, 2000.

[3] A. J. Nozik, " Quantum dot solar cells," Physica E: Low-dimensional Systems and Nanostructures, vol. 14, pp. 115-120, 2002.

[4] W. Shockley and H. J. Queisser, " Detailed Balance Limit of Efficiency of pn Junction Solar Cells," J. Appl. Phys. vol. 32, no. 3, pp. 510-519, 1961.

[5] Y. Okada, N. J. Ekins-Daukes, T. Kita, R. Tamaki, M. Yoshida, A. Pusch, O. Hess, C. C. Phillips, D. J. Farrell, K. Yoshida, N. Ahsan, Y. Shoji, T. Sogabe, and J.-F. Guillemoles, " Intermediate band solar cells: Recent progress and future directions," Applied Physics Reviews, vol. 2, no. 2, pp. 021302-021348, 2015.

[6] M. A. Green, " Third Generation Photovoltaics: Advanced Solar, Electricity Generation, " Springer Berlin Heidelberg, vol. 12, 2003.

[7] W. Jiang, M. W. Zhiming, " Quantum Dot Solar Cells, Lecture Notes in Nanoscale Science and Technology, " Editors Springer, vol. 15, 2014.

[8] O. L. Lazarenkova and A. A. Balandin, " Miniband formation in a quantum dot crystal, " J. Appl. Phys, vol. 89, no. 10, pp. 5509-5515, 2001.

[9] Q. Shao, A. A. Balandin, A. I. Fedoseyev and M. Turowski, " Intermediate-band solar cells based on quantum dot supracrystals, " Appl. Phys. Lett, vol.91, pp. 163503-3, 2007.

[10] M. Y. Levy, C. Honsberg, A. Marti and A. Luque, " Quantum dot intermediate band solar cell material systems with negligible valence band offsets, " Conference Record of the Thirty-first IEEE Photovoltaic Specialists Conference, 2005.

[11] C. G. Bailey, D. V. Forbes, R. P. Raffaelle, and S. M. Hubbard, " Near 1 V open circuit voltage InAs/GaAs quantum dot solar cells, " Appl. Phys. Lett, vol. 98, pp. 163105-3, 2011.

[12] V. Aroutiounian, S. Petrosyan, A. Khachatryan, and K. Touryan, " Quantum dot solar cells, " J. Appl. Phys, vol. 89, no. 4, pp. 2268-2271, 2001.

[13] A. Imran, J. Jiang, D. Eric, M. N. Zahid, M. Yousaf, M. Ahmad, S. A. Hassan, " Efficiency Enhancement through Flat Intermediate Band in Quantum Dot Solar Cell, " Results in Physics, vol. 10, pp. 241-247, 2018.

[14] D. A. McQuarrie, " The Kronig-Penney Model: A Single Lecture Illustrating the Band Structure of Solids, " Springer-Verlag New York, Inc, vol. 1, no. 1, pp. 01003-5, 1996.

[15] Q. Deng, X. Wang, C. Yang, H. Xiao, C Wang, H. Yin, Q. Hou, J. Li, Z. Wang, and X. Hou, " Theoretical study on $In_xGa_{1-x}N/GaN$ quantum dots solar cell, " Physica B, vol. 406, pp. 73-76, 2011.

[16] Q. Zhang and W. Wei, " Single intermediate-band solar cells of InGaN/InN quantum dot supracrystals, " Appl. Phys. A, vol. 113, no. 1, pp. 75-82, 2013.

[17] N. Ben Afkir, E. Feddi, F. Dujardin, M. Zazoui and J. Meziane, " Photovoltaic conversion efficiency of InN/InxGa1-xN quantum dot intermediate band solar cells, " Physica B, vol. 534, pp. 10-16, 2018.

[18] W. Hu, M. F. Budiman, M. Igarashi, M. Y. Lee, Y. Li, and S. Samukawa, " Modeling miniband for realistic silicon nanocrystal array, " Mathematical and Computer Modelling, vol. 58, pp. 306-311, 2013.

[19] A. El-Maaty M. Aly and A. " Nasr, Theoretical performance of solar cell based on mini-bands quantum dots, " Journal of Applied Physics, vol. 115, pp. 114311-9, 2014.

[20] P. Y. Yu, M. Cardona, " Fundamentals of Semiconductors, " Springer, Berlin, 1998.

[21] Y. P. Varshni, " Temperature dependence of the energy gap in semiconductors, " Physica E, vol. 34, pp. 148-154, 1967.

[22] I. Vurgftman, J. R. Meyer, " Band parameters for nitrogen-containing semiconductors, " J .Appl. Phys, vol. 94, no. 6, pp. 3675-3696, 2003.

[23] W. van Roosbroeck and W. Shockley, " Photon-Radiative Recombination of Electrons and Holes in Germanium, " Phys.Rev, vol. 94, pp. 1558-1560, 1954.

[24] G. Bastard, " Theoretical investigations of superlattice band structure in the envelope-function approximation, " Phys. Rev. B, vol. 25, no. 12, pp. 7584-7597, 1982.

[25] A. Luque, A. Martí, N. López, " Experimental analysis of the quasi-Fermi level split in quantum dot intermediate-band solar cells, " Appl. Phys. Lett, vol. 87, no. 8, pp. 083503-3, 2005.

[26] P. Rinke, M. Winkelkemper, A. Qteish, D. Bimberg, J. Neugebauer, and M. Sheffer, " Consistent set of band parameters for the group-III nitrides AlN, GaN, and InN, " Phys. Rev. B, vol. 77, pp. 075202-15, 2008.